RESEARCH ARTICLE SUMMARY

GENOMIC DUPLICATIONS

Exploring whole-genome duplicate gene retention with complex genetic interaction analysis

Elena Kuzmin*, Benjamin VanderSluis*, Alex N. Nguyen Ba, Wen Wang, Elizabeth N. Koch, Matej Usaj, Anton Khmelinskii, Mojca Mattiazzi Usaj, Jolanda van Leeuwen, Oren Kraus, Amy Tresenrider, Michael Pryszlak, Ming-Che Hu, Brenda Varriano, Michael Costanzo, Michael Knop, Alan Moses, Chad L. Myers†, Brenda J. Andrews†, Charles Boone†

INTRODUCTION: Whole-genome duplication (WGD) events are pervasive in eukaryotes, shaping the genomes of simple single-celled organisms, such as yeast, as well as those of more complex metazoans, including humans. Most duplicated genes are eliminated after WGD because one copy accumulates deleterious mutations, leading to its loss. However, a significant proportion of duplicates persists, and factors that result in duplicate gene retention are poorly understood but critical for understanding the evolutionary forces that shape genomes.

RATIONALE: Quantifying the functional divergence of paralog pairs is of particular interest because of the strong selection against functional redundancy. Negative genetic interactions identify functional relationships between genes and provide a means to directly capture the functional relationship between duplicated genes. Genetic interactions occur when the phenotype associated with a combination of mutations in two or more different genes deviates from the expected combined effect of the individual mutations. A negative genetic interaction refers to a combination of mutations that generates a stronger fitness defect than expected, such as synthetic lethality. Here, we used systematic analysis of digenic and trigenic interaction profiles to assess the functional relationship of retained duplicated genes.

ON OUR WEBSITE

Read the full article at https://dx.doi.org/10.1126/science.aaz5667

RESULTS: To map both digenic and trigenic interactions of duplicated genes, we profiled query strains carrying single-deletion mutations and the corresponding double-deletion mutations for 240 different dispensable paralog pairs originating from the yeast WGD event. In total, we tested ~550,000 double and ~260,000 triple mutants for genetic interactions, and identified ~4700 negative digenic interactions and ~2500 negative trigenic interactions. We quantified the trigenic interaction fraction, defined as the ratio of negative trigenic interactions to the total number of interactions associated with the paralog pair. The distribution of the resulting trigenic interaction fractions was distinctly bimodal, with two-thirds of paralogs exhibiting a low trigenic interaction fraction (diverged paralogs) and one-third showing a high trigenic interaction fraction (functionally redundant paralogs). Paralogs with a high trigenic interaction fraction showed a relatively low asymmetry in their number of digenic interactions, low rates of protein sequence divergence, and a negative digenic interaction within the gene pair.

We correlated position-specific evolutionary rate patterns between paralogs to assess constraints acting on their evolutionary trajectories. Paralogs with a high trigenic interaction fraction showed more correlated evolutionary rate patterns and thus were more evolutionarily constrained than paralogs with a low trigenic interaction fraction. Computational simulations that modeled duplicate gene evolution revealed that as the extent of the initial entanglement (overlap of functions) of paralogs increased, so did the range of functional redundancy at steady state. Thus, the bimodal distribution of the trigenic interaction fraction may reflect that some paralogs diverged, primarily evolving distinct functions without redundancy, while others converged to an evolutionary steady state with substantial redundancy due to their structural and functional entanglement.

CONCLUSION: We propose that the evolutionary fate of a duplicated gene is dictated by an interplay of structural and functional entanglement. Paralog pairs with high levels of entanglement are more likely to revert to a singleton state. In contrast, unconstrained paralogs will tend to partition their functions and adopt divergent roles. Intermediately entangled paralog pairs may partition or expand nonoverlapping functions while also retaining some common, overlapping functions, such that they can both adopt paralog-specific roles and maintain functional redundancy at an evolutionary steady state. ■

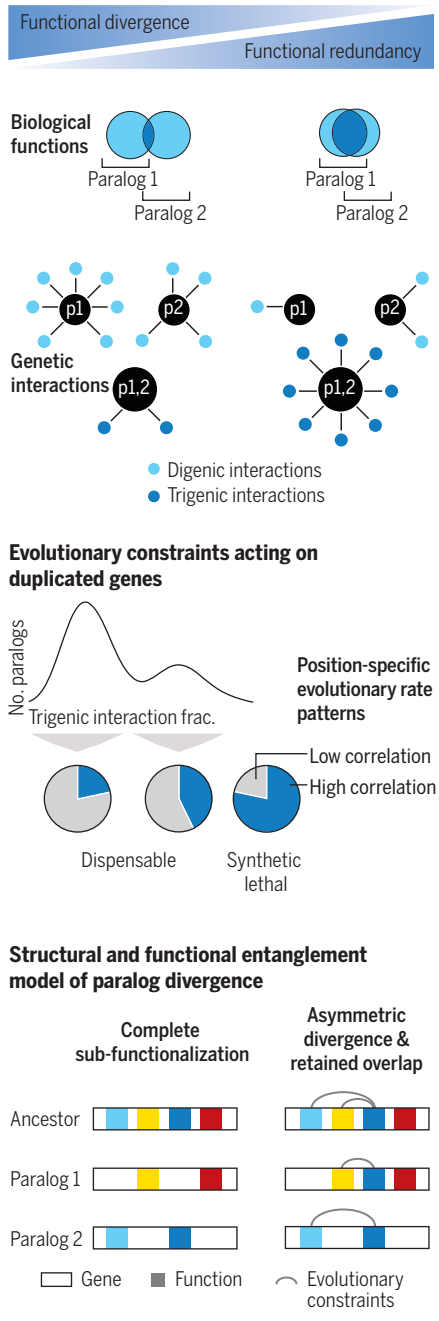

Complex genetic interaction analysis of duplicated genes. The trigenic interaction fraction, which incorporates digenic and trigenic interactions, captures the functional relationship of duplicated genes and follows a bimodal distribution. Paralogs with a high trigenic interaction fraction are under evolutionary constraints reflecting their structural and functional entanglement.

The list of author affiliations is available in the full article online.
*These authors contributed equally to this work.
†Corresponding author. Email: charlie.boone@utoronto.ca (C.B.); brenda.andrews@utoronto.ca (B.J.A.); chadm@umn.edu (C.L.M.)
Cite this article as E. Kuzmin *et al.*, *Science* **368**, eaaz5667 (2020). DOI: 10.1126/science.aaz5667

RESEARCH ARTICLE

GENOMIC DUPLICATIONS

Exploring whole-genome duplicate gene retention with complex genetic interaction analysis

Elena Kuzmin[1,2]*†, Benjamin VanderSluis[3]*, Alex N. Nguyen Ba[4,5]‡, Wen Wang[3], Elizabeth N. Koch[3], Matej Usaj[1], Anton Khmelinskii[6]§, Mojca Mattiazzi Usaj[1], Jolanda van Leeuwen[1]¶, Oren Kraus[1,2], Amy Tresenrider[7], Michael Pryszlak[1,2], Ming-Che Hu[1], Brenda Varriano[1], Michael Costanzo[1], Michael Knop[6,8], Alan Moses[4,5,9], Chad L. Myers[3]#, Brenda J. Andrews[1,2]#, Charles Boone[1,2]#

Whole-genome duplication has played a central role in the genome evolution of many organisms, including the human genome. Most duplicated genes are eliminated, and factors that influence the retention of persisting duplicates remain poorly understood. We describe a systematic complex genetic interaction analysis with yeast paralogs derived from the whole-genome duplication event. Mapping of digenic interactions for a deletion mutant of each paralog, and of trigenic interactions for the double mutant, provides insight into their roles and a quantitative measure of their functional redundancy. Trigenic interaction analysis distinguishes two classes of paralogs: a more functionally divergent subset and another that retained more functional overlap. Gene feature analysis and modeling suggest that evolutionary trajectories of duplicated genes are dictated by combined functional and structural entanglement factors.

Most eukaryotic genomes, including the human genome, contain a substantial fraction of duplicated genes (*1*–*7*). Gene duplication is generated by two main mechanisms: segmental duplication (small-scale duplication) due to error-prone DNA replication, and simultaneous duplication of all genomic segments (whole-genome duplication) due to a variety of polyploidy events (*3*, *8*). Gene duplication provides a source of new genes (*9*), and duplicate retention may lead to the development of specialized functional modules involving paralogous proteins through "subfunctionalization," which promotes biological complexity (*10*). Nonetheless, after duplication most paralogs are eliminated from the genome because the functional redundancy of duplicated genes is evolutionarily unstable, as one gene copy may accumulate intrinsically deleterious mutations and be removed from the genome by selection (*11*). However, a significant fraction of duplicates has been retained over the course of evolution. Thus, understanding the molecular mechanisms that underlie duplicate gene retention may provide insights into the evolutionary forces that shape genomes.

About 100 million years ago, the budding yeast *Saccharomyces cerevisiae* arose from a whole-genome duplication (WGD) event, and, after a massive gene loss, retained 551 duplicate gene pairs (*6*, *7*, *12*). Quantifying the functional divergence of each paralog pair is of particular interest because of the strong selection against functional redundancy. Paralog functional divergence has been estimated by the rates of evolutionary divergence of coding and regulatory regions (*6*, *12*–*14*), Gene Ontology (GO) semantic distance (*15*–*17*), metabolic flux analysis (*18*, *19*), similarity of gene expression profiles (*3*, *10*, *20*–*23*), changes in the encoded protein abundance of one sister upon perturbation of another (*24*), and analysis of similarity of partners within the protein-protein interaction network (*25*).

Genetic interaction analysis provides a powerful means to directly capture the functional relationship between duplicated genes. Genetic interactions occur when a combination of mutations in different genes results in an unexpected phenotype, deviating from a model based on the integration of the individual mutant phenotypes. A negative genetic interaction occurs when a combination of mutations leads to a more severe fitness defect than expected (*26*). An extreme example of a negative digenic interaction is synthetic lethality, which occurs when two mutations, neither of which is lethal on its own, combine to generate an inviable double-mutant phenotype (*27*, *28*). Negative genetic interactions often occur between genes that impinge on a common essential function. A positive genetic interaction occurs when a combination of mutations results in a phenotype that is less severe than expected from the phenotypes associated with the single mutants. For example, digenic suppression is observed when a double mutant exhibits a greater fitness than the sickest single mutant (*29*). A previous global digenic interaction network in yeast identified ~550,000 negative and ~350,000 positive genetic interactions (*30*). The profile of genetic interactions for a specific query gene provides a quantitative measure of function (*31*, *32*), and a network based on genetic interaction profile similarity reveals a hierarchy of functional modules, including pathways and complexes, bioprocesses, and cellular compartments (*30*).

A systematic analysis of the digenic interactions between duplicated gene pairs in yeast revealed functional redundancy, whereby ~30% of pairs interacted (relative to ~3.6% for random gene pairs) (*33*–*37*). However, this observation may indicate that the overall contribution of duplicate retention to the ability of an organism to tolerate mutations, known as mutational robustness, is relatively low because total functional compensation is only observed for a minor fraction of duplicates (*38*). Mechanisms that drive duplicate retention may be influenced by gene dosage effects or by functional divergence through asymmetric evolution (*33*). Retention of duplicates may result from subfunctionalization, such that duplicates degenerate in some of their function differentially and result in a pair of genes that function fully as the single ancestral copy; this outcome is postulated by the duplication-degeneration-complementation model (*39*). Evidence of functional partitioning of ancestral functions includes but is not limited to biochemical function (*40*), gene expression regulatory elements (*22*), and subcellular localization patterns (*41*).

Here, we expanded upon the use of genetic interaction profiles to capture the functional relationship of duplicated genes. We compared trigenic interactions for double-mutant query strains deleted for both members of nonessential paralog pairs to the corresponding digenic interaction profiles for each single-mutant sister gene, and we quantified a spectrum of functional redundancy among paralogs. A correlative analysis of the gene features suggests that the evolutionary trajectories of retained duplicated genes can be driven by genes encoding functionally and structurally

[1]Donnelly Centre, University of Toronto, Toronto, Ontario M5S 3E1, Canada. [2]Department of Molecular Genetics, University of Toronto, Toronto, Ontario M5S 3E1, Canada. [3]Department of Computer Science and Engineering, University of Minnesota, Minneapolis, MN 55455, USA. [4]Department of Cell and Systems Biology, University of Toronto, Toronto, Ontario, Canada. [5]Center for Analysis of Evolution and Function, University of Toronto, Toronto, Ontario, Canada. [6]Zentrum für Molekulare Biologie der Universität Heidelberg (ZMBH), DKFZ-ZMBH Alliance, 69120 Heidelberg, Germany. [7]Department of Molecular and Cell Biology, University of California, Berkeley, CA, USA. [8]Cell Morphogenesis and Signal Transduction, German Cancer Research Center (DKFZ), 69120 Heidelberg, Germany. [9]Department of Ecology and Evolutionary Biology, University of Toronto, Toronto, Ontario, Canada.
*These authors contributed equally to this work.
†Present address: Rosalind and Morris Goodman Cancer Research Centre, McGill University, Montreal, Quebec H3A 1A3, Canada.
‡Present address: Department of Organismic and Evolutionary Biology, Harvard University, Cambridge, MA, USA.
§Present address: Institute of Molecular Biology, Mainz, Germany.
¶Present address: Center for Integrative Genomics, University of Lausanne, Lausanne, Switzerland.
#Corresponding author. Email: charlie.boone@utoronto.ca (C.B.); brenda.andrews@utoronto.ca (B.J.A.); chadm@umn.edu (C.L.M.)

constrained proteins, which we refer to as "entangled."

Mapping trigenic interactions for duplicated genes

We constructed 240 double-mutant query yeast strains, each deleted for a pair of nonessential WGD paralog genes (tables S1 to S4). These are dispensable paralog pairs and represent 44% (240/551) of unique WGD paralog pairs (*12*), a number of which were not included because the pair was either essential or refractory to double-mutant query strain construction (*42*). Using colony size as a proxy for cell fitness, we measured the growth phenotypes of the set of 240 double-mutant query strains and the corresponding 480 single mutants (table S5) (*42*), which correlated well with previous large-scale measurements of single-mutant fitness (Pearson correlation coefficient $r = 0.51$, $P = 3 \times 10^{-30}$) and double-mutant fitness ($r = 0.72$, $P = 2 \times 10^{-23}$) (*30*) (fig. S1, A to D).

We used the set of single- and double-mutant query strains to score digenic and trigenic interactions, respectively, using trigenic synthetic genetic array analysis (τ-SGA) (Fig. 1). We crossed the queries to a diagnostic array of nonessential gene deletion mutants and essential gene mutants, carrying temperature-sensitive alleles, which span all major cellular processes and cover ~1200 genes representing ~20% of the yeast genome (*37*). In total, we examined 537,911 double and 256,861 triple mutants for genetic interactions. Query strains deleted for an individual paralog gene were screened for digenic interactions, and double-mutant query strains deleted for both paralogs were screened for trigenic interactions in two replicate screens with four colonies per screen (fig. S2, A to C) (*37*). Negative and positive interactions were quantified for digenic and trigenic interactions (*30*, *32*), which were determined from validation of trigenic interactions of the *CLN1-CLN2* double-mutant query, as previously described (*37*). This resulted in an estimated recall (sensitivity) of ~60% and a precision of ~75% (*37*). Additionally, we used replicate screens to independently estimate the false discovery rate (FDR) as a function of recall, which resulted in a consistent estimate of >75% precision (<25% FDR) (fig. S2D).

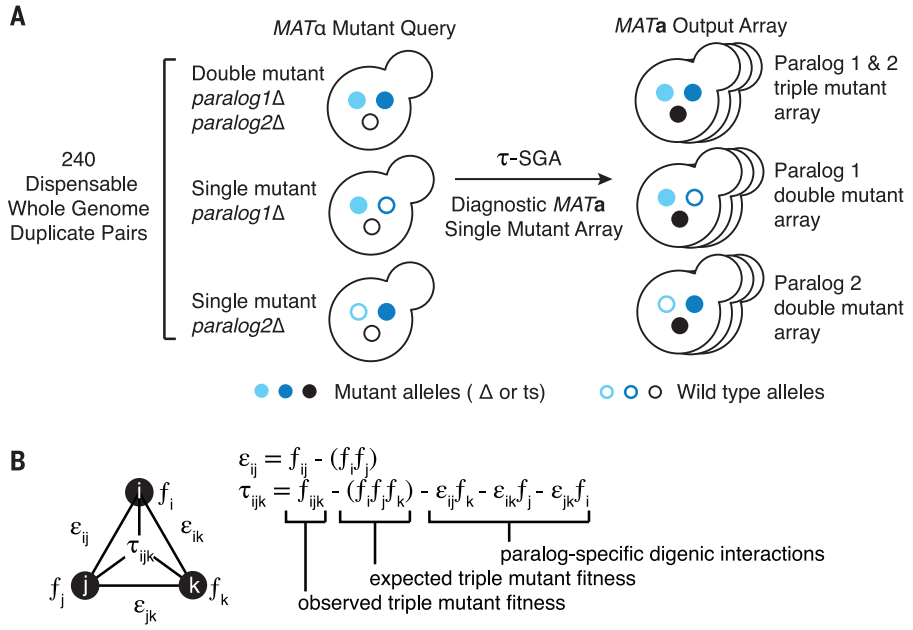

Fig. 1. Trigenic synthetic genetic array (τ-SGA) analysis for paralogs. (**A**) An illustration of the τ-SGA experimental approach in which a query set of 240 dispensable paralog pairs originating from whole-genome duplication (WGD) in yeast was screened for trigenic interactions. Three types of screens were carried out in parallel, whereby triple-mutant fitness was estimated by crossing a double-mutant query strain deleted for both paralogs (light and dark blue solid circles) into a diagnostic array of single mutants (black solid circles) (*37*). After induction of meiosis in heterozygous triple mutants, sequential replica-pinning steps are used to select haploid triple-mutant progeny. Single-mutant control query strains are screened in parallel to estimate paralog-specific double-mutant fitness. (**B**) We used the τ-SGA scoring method to identify trigenic interactions quantitatively by combining double- and triple-mutant fitness estimates derived from colony size measurements (*37*). The digenic interaction score is expressed as ε_{ij}, where f_{ij} is the observed double-mutant fitness, and the expected double-mutant fitness is expressed as the product of single-mutant fitness estimates $f_i f_j$. The trigenic interaction score is expressed as τ_{ijk}, where f_{ijk} is the observed triple-mutant fitness and $f_i f_j f_k$ is the triple-mutant fitness expectation expressed as the product of three single-mutant fitness estimates.

This analysis identified 4650 negative and 2547 positive digenic interactions, as well as 2466 negative and 2091 positive trigenic interactions (tables S1, S2, and S4). About one-third of negative and one-fourth of positive trigenic interactions were of the "novel" class, identifying connections that were not observed in their corresponding digenic interaction network (Fig. 2). Indeed, for 129 paralog pairs, the corresponding single genes displayed only sparse digenic interaction profiles on the global genetic interaction network (*30*) (table S6). However, they exhibited more novel trigenic interactions (~40% negative and ~31% positive trigenic interactions) than average, indicating that paralog pair trigenic interactions expanded the known global genetic interaction network. The remaining two-thirds of negative and three-fourths of positive trigenic interactions overlapped a previously identified digenic interaction and thus represent a "modified" class of trigenic interactions (Fig. 2). Paralogs with more negative trigenic interactions than digenic interactions showed predominantly novel and modified negative trigenic interactions, which overlapped exclusively with negative digenic interactions indicating functional redundancy (fig. S3A).

Genetic interaction profiles highlight functional divergence of duplicated genes

The functional relationship between paralogs should be captured by their negative genetic interactions. Consistent with previous observations (*32*, *33*), we observed that duplicates showed fewer negative digenic interactions than singletons (Wilcoxon rank-sum test, $P = 6 \times 10^{-8}$; fig. S3B), which is suggestive of a general trend in which paralogs retain functional redundancy. We predicted that highly divergent gene pairs should exhibit a relatively high number of paralog-specific negative digenic interactions (Fig. 3). In contrast, functionally overlapping paralogs should be biased toward trigenic interactions and should display few paralog-specific interactions (Fig. 3). To assess this possibility, we computed the trigenic interaction fraction, defined as the ratio of negative trigenic interactions to the total number of all negative interactions (digenic and trigenic) associated with the paralog pair (Fig. 3).

From this analysis, we observed that double mutants involving duplicates showed a range of trigenic and digenic interaction degrees. This indicated that complex genetic interactions may reveal their functional redundancy (fig. S3B). For example, *SKI7-HBS1* is a paralog pair that showed a relatively low trigenic interaction fraction (Fig. 3). Although the *SKI7* and *HBS1* gene products both recognize stalled ribosomes and initiate mRNA degradation, they do so in a different manner (*43*). Ribosomes that stall upon encountering an in-frame stop

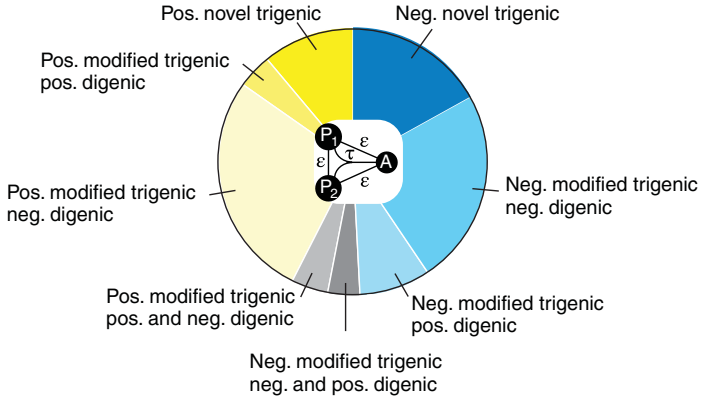

Fig. 2. Distribution of different types of trigenic interactions for paralogs. The different types of trigenic interactions for all paralogs are compared in a pie chart. Negative [(τ or ε) < −0.08, P < 0.05] and positive [(τ or ε) > 0.08, P < 0.05] genetic interactions are shown in blue and yellow, respectively. A trigenic interaction between a double-mutant query and the array strain is called "novel" (dark blue/dark yellow) if there is no significant digenic interaction between either single-mutant control query and the array strain or between the query gene pair. Trigenic interactions that overlap with one or more negative or positive digenic interactions are called "modified" and are further classified by the type of digenic interaction. All trigenic interactions of double-mutant query strains that show a negative or a positive digenic interaction between the members of a query gene pair (P_1-P_2) ($|\varepsilon|$ > 0.08, P < 0.05) are considered "modified." Interactions may be further classified by digenic interactions (if any) between a single-mutant query control strain and the array strain (P_1 and/or P_2-A negative, P_1 and/or P_2-A positive). Digenic interactions of the same sign are in medium blue/yellow, digenic interactions of the opposite sign are in light blue/yellow, and mixed positive and negative digenic interactions are depicted in different shades of gray according to whether their modified trigenic interactions are positive or negative.

codon at the 3′ end of a transcript are recognized by Ski7, which in turn recruits the RNA exosome (*44*). In contrast, ribosomes stalled within the coding region of a transcript, possibly because of an unusual structural conformation or damage in the mRNA, are recognized by Hbs1, which initiates mRNA cleavage in an RNA exosome–independent manner (*45*). Our model (Fig. 3) predicts that the digenic interaction profiles of the paralogs should reflect their independent function. Indeed, *SKI7* showed digenic interactions with genes involved in mRNA 3′ end protection and 5′-3′ mRNA decay, such as *PAT1* and *LSM1*, whereas *HBS1* interacted with numerous genes involved in ribosome biogenesis and recycling. Thus, the low trigenic interaction fraction of the *SKI7-HBS1* gene pair (Fig. 3) appears to reflect the functional divergence of these paralogs (*39*, *40*, *43*).

Conversely, the *MRS3-MRS4* duplicate pair showed a high trigenic interaction fraction (~0.85) (Fig. 3). These paralogs are members of the eukaryotic-specific mitochondrial carrier family, which transports compounds, including nucleotides, amino acids, carboxylates, small inorganic ions, and vitamins, across the inner mitochondrial membrane linking the cytosolic and mitochondrial biochemical pathways (*46*). *MRS3* and *MRS4* encode highly similar mitochondrial carrier proteins with high affinity for Fe^{2+}, which they transport across the inner mitochondrial membrane (*47*). The corresponding vertebrate homolog, mitoferrin, is involved in erythropoiesis by maintaining mitochondrial iron homeostasis (*48*). The *MRS3-MRS4* trigenic interactions involved genes related to cell redox homeostasis, such as *GRX3*, *TSA1*, and *TRX3*. The processes that regulate Fe^{2+} homeostasis are important components of the cellular defense mechanism against oxidative damage. Indeed, the *MRS3-MRS4* trigenic interactions were also enriched for genes involved in DNA replication and repair, including genes encoding members of the Rad51-Rad57 complex (*RAD51*, *RAD54*, *RAD55*, *RAD57*), the Rad5-Rad6-Rad18 complex (*RAD5*), the DNA replication factor C complex (*CTF8*, *CTF18*), the MRX complex (*MRE11*, *XRS2*), the Holliday junction resolvase complex (*MUS81*, *MMS4*), and the nucleotide-excision repair factor 3 complex (*TFB1*, *SSL1*) (*49*). Together these examples illustrate how the trigenic interaction fraction may reflect the degree of functional overlap of paralogs.

Distribution of trigenic interaction fraction among retained paralog pairs

In total, we measured the trigenic interaction fraction for 161 paralog pairs that showed at least six total trigenic or digenic interactions (table S7). These paralog pairs displayed a range of trigenic interaction fraction values (Fig. 4A) that showed a distinctly bimodal distribution, with 114 paralog pairs exhibiting a relatively low trigenic interaction fraction (below 0.4) while a smaller subset of 47 paralogs displayed a higher trigenic interaction fraction (above 0.4). This finding suggests that comparison of digenic and trigenic interaction profiles is an effective way to differentiate paralog pairs and can provide insight into the extent of functional overlap between members of a given duplicated gene pair (Fig. 4A and table S7). This distribution of trigenic interaction did not differ for subsets of duplicated genes that originated by distinct mechanisms, such as ohnologs, which originated from WGD, or homeologs, which originated from hybridization between species (*42*, *50*). We confirmed that the genetic interaction profiles we generated are robust to array size, in that we observed a significant correlation for the trigenic interactions obtained from the diagnostic array and the genome-wide array, which were derived from screening 11 double mutants with their single-mutant control query strains in two replicates each (fig. S4). The strength of correlation between replicates was not affected appreciably with decreasing stringency for either digenic or trigenic interactions (fig. S2, A to C), indicating that our conclusions are not dependent on an interaction score threshold. The remaining 79 paralog pairs, representing about one-third of all screened pairs, were characterized by sparse genetic interaction profiles. These paralogs span a diverse set of biological processes and tend to belong to larger gene families (one-sided t test, P = 0.04; table S9), which may confer higher-order redundancy and reduce second- and third-order genetic interactions.

Trigenic interaction fraction, digenic interaction profiles, and paralog properties

The trigenic interaction fraction of paralog pairs was also associated with several fundamental physiological and evolutionary properties (Fig. 4B and tables S5, S7, and S10). Paralogs with a high trigenic interaction fraction tend to exhibit low asymmetry with respect to their number of digenic interactions. The asymmetry score measures whether the digenic profile of one paralog is composed of substantially more interactions than its corresponding duplicate, and it correlates with divergent evolution of paralog gene sequences (*33*). Consistent with this observation, a high trigenic interaction fraction also correlated with relatively low rates of protein sequence divergence (Fig. 4B). We also observed a high trigenic interaction fraction in paralogs whose double mutant showed a negative digenic interaction, which is often associated with functionally related genes (Fig. 4B) (*30*, *37*).

Conversely, paralogs with a low trigenic interaction fraction often showed a high asymmetric score for their digenic degrees (Fig. 4B). Consistent with our hypothesis that a low trigenic fraction is indicative of functional divergence (Figs. 3 and 4A), a high asymmetry score may reflect that one paralog has evolved a specialized role. For example, a paralog displaying relatively few digenic interactions under standard conditions may only be expressed and functional under a different environmental condition or during a specialized developmental program. Indeed, in the case of four

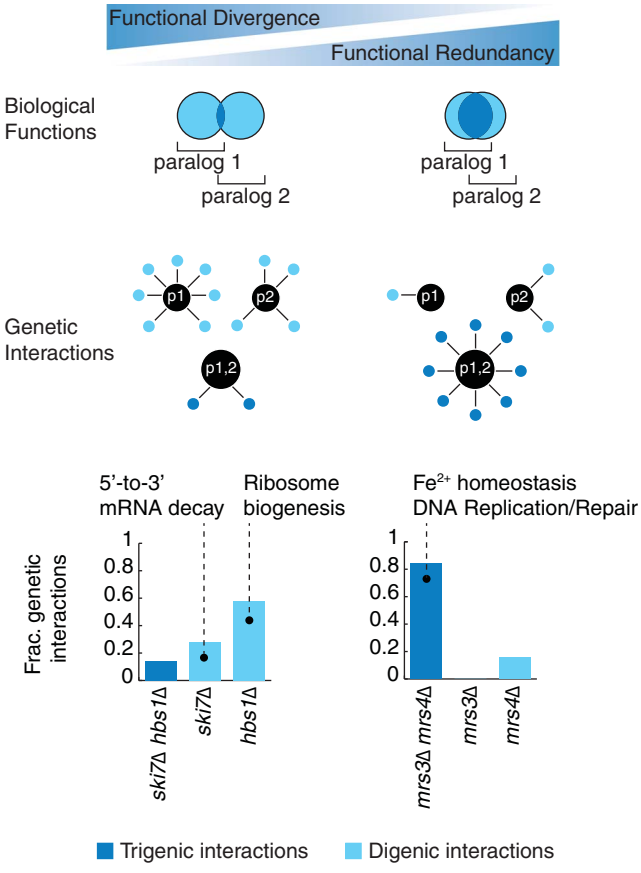

Fig. 3. Mapping the functional relationship of paralogs through their digenic and trigenic interactions. This schematic depicts highly divergent paralogs with little functional overlap and functionally redundant paralogs with extensive functional overlap, as represented by the Venn diagrams. Diverged paralogs are predicted to exhibit many digenic interactions, indicative of their paralog-specific functions and few trigenic interactions, whereas functionally redundant paralogs are expected to show sparse digenic interactions and numerous trigenic interactions, indicative of their functional overlap. Divergent paralogs such as *SKI7-HBS1* behave in a manner consistent with the expectation and display fewer trigenic than digenic interactions. However, functionally redundant paralogs such as *MRS3-MRS4* display a higher fraction of trigenic interactions with a corresponding drop in the fraction of paralog-specific digenic interactions. The fraction of different types of genetic interactions is illustrated using bar graphs. The fraction of total genetic interactions attributed to the trigenic interactions associated with a *par1*Δ *par2*Δ double-mutant query, deleted for both paralogs, is shown as a dark blue bar; the fraction of digenic interactions associated with each paralog single-deletion mutant, *par1*Δ or *par2*Δ, is shown as a light blue bar.

asymmetric paralog pairs, expression of the low-degree sister was induced during sporulation, a meiotic developmental program that cells enter in response to a low-carbon and low-nitrogen environment. Specifically, *GIS1* in paralog pair *GIS1-RPH1*, *HES1* in *HES1-KES1*, *ECI1* in *ECI1-DCI1*, and *DON1* in *DON1-CUE5* showed higher meiotic gene expression (table S11) (*51*). For another seven asymmetric paralog pairs, the low-degree paralog was required for filamentous growth (*52*), and for another 15 asymmetric pairs, the gene expression of the low-degree sister was induced under glucose starvation (table S11) (*53*). In total, 22 of 63 asymmetric pairs (~35%) have a paralog that may have been retained for function in a different condition or during a specialized program (table S11).

The retention of gene duplicates may also be related to gene dosage (*54*). For example, some duplicates appear to be maintained as a result of selection for high levels of expression, as in the case of metabolic genes that provide high enzymatic flux (*18*). WGD events also enable maintenance of stoichiometric balance of protein complex members, consistent with the high rate of duplication among components of the ribosome (*35*). Dosage duplicates are associated with a severe fitness defect when either one of the paralogs is deleted, as well as a greater digenic interaction profile similarity than other duplicates, indicating that they have retained functional redundancy (*33*, *38*). Because dosage duplicates should have substantial functional redundancy, we reasoned that they might also tend to have a higher trigenic interaction fraction. Although the paralogs with a greater digenic interaction profile similarity also tend to have a higher trigenic interaction fraction (Fig. 4C), potential dosage duplicates (*33*) were found within both the high and low trigenic interaction fraction distributions (table S10). Thus, the functional redundancy associated with the subset of paralogs with a higher trigenic interaction fraction is probably not driven solely by dosage mechanisms.

The evolution of regions important for protein localization may lead to differential subcellular localization of some paralogous proteins and may play a role in their retention by enabling specific paralog functions in distinct parts of the cell (*41*, *55*). However, because on average duplicated genes do not appear to evolve a relocalization more frequently than singletons, this may not represent a major mechanism driving paralog retention (*56*). We observed that paralogs with different subcellular localization patterns tended to show a modestly higher trigenic interaction fraction than those with the same subcellular localization patterns (Wilcoxon rank-sum test, $P < 0.05$), which suggests that differentially localized paralogs may retain some functional overlap.

Defining paralog function in terms of trigenic interactions

To characterize the roles of paralog pairs with overlapping functions, we mapped their trigenic interactions onto the global digenic interaction profile similarity network (*30*) (Fig. 5A). Using this approach, trigenic interactions associated with paralog pairs that have a relatively high trigenic interaction fraction can be examined for enrichment within defined bioprocesses. For example, the *sbe2*Δ *sbe22*Δ double mutant showed few paralog-specific interactions and numerous trigenic interactions, with a trigenic interaction fraction of ~0.69 (table S7). The proteins encoded by the *SBE2-SBE22* pair share ~51% amino acid sequence identity and have relatively well-characterized functions in the transport of cell wall components from the Golgi to the cell surface (*57*). The *SBE2-SBE22* negative trigenic interactions involved genes enriched for GO annotations related to vesicle-mediated transport and cell wall organization (Fig. 5B) and include interactions with an ARF-like small guanosine triphosphatase (GTPase) secretion pathway (*ARL1*, *ARL3*, *SYS1*, *YPT6*), the exocyst (*SEC4*), and the chitin biosynthesis pathway (*CHS5*, *CHS6*).

Previously, we showed that trigenic interactions, like digenic interactions, are functionally informative and are enriched among genes annotated to the same biological process (*37*). Mapping paralog trigenic interaction profiles onto the global digenic interaction profile similarity network enables the functional annotation of previously uncharacterized paralogs. For example, *ECM13-YJR115W* showed a trigenic interaction fraction of 0.77 with 12 negative digenic and 40 negative trigenic interactions, suggesting high functional redundancy (fig. S5A and table S7). These paralogs are fungal-specific and share 39% identity and 70% similarity at the amino acid sequence level. The genes that constitute the *ECM13-YJR115W* trigenic interaction profile were positioned mainly within the mitosis and DNA replication and repair clusters on the global digenic profile network (Fig. 5C). The *ECM13-YJR115* trigenic interaction profile is correlated to the digenic interaction profiles

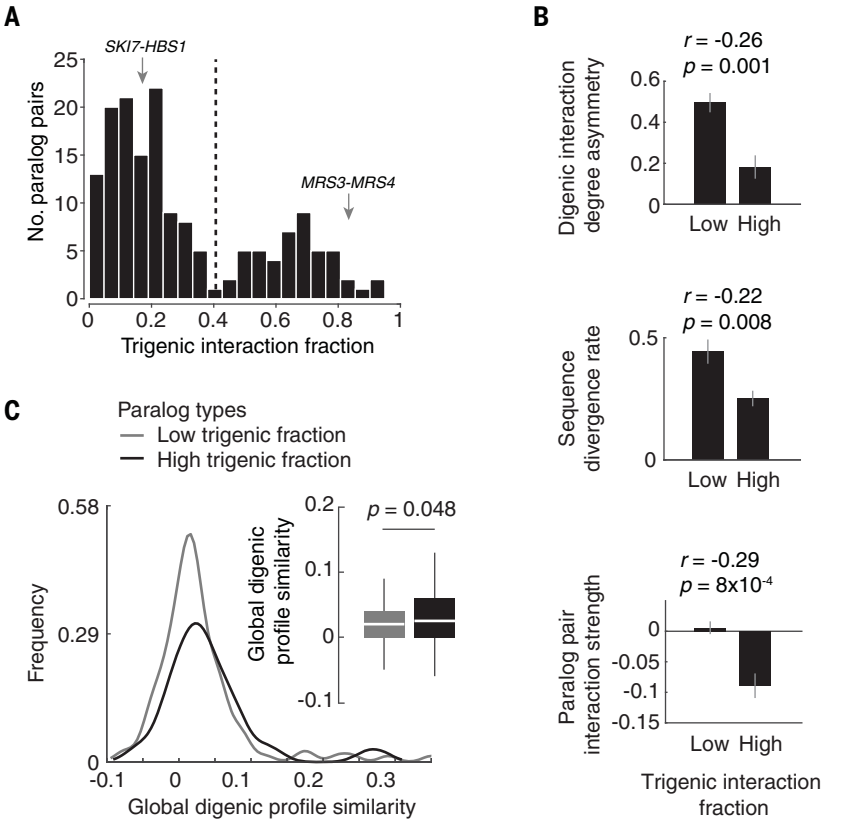

Fig. 4. The trigenic interaction fraction correlates with fundamental physiological and evolutionary properties. (**A**) Negative trigenic interaction fraction distribution of screened paralogs, (τ or ε) < −0.08, P < 0.05; paralogs with at least six trigenic or digenic interactions in one of the screens are considered. Representative examples of paralogs with a low (*SKI7-HBS1*) and high (*MRS3-MRS4*) trigenic interaction fraction are marked with an arrow. (**B**) Physiological and evolutionary properties for paralogs characterized by varying fraction of trigenic interactions. Spearman correlation coefficients (r) and associated P values are measures of the strength of the correlation between the trigenic interaction fraction and the three features being examined: digenic interaction degree asymmetry, sequence divergence rate, and paralog pair interaction strength. The correlation was measured on the entire dataset. The bar plots serve to visualize the trend, in which a trigenic interaction fraction cutoff of 0.4 was used to identify paralogs with low and high trigenic interaction fraction, based on negative interactions (τ or ε) < −0.08, P < 0.05. Means of specified features are shown; error bars denote SEM. (**C**) The distribution of global digenic profile correlation similarity (*30*) was compared for paralogs with high and low trigenic interaction fraction. A trigenic interaction fraction cutoff of 0.4 was used as in (B). Box plots serve to summarize the data of the distributions. Analyses are restricted to paralogs with at least six total trigenic or digenic interactions in one of the screens. Significance was assessed using one-tailed Wilcoxon rank-sum test.

of *CCT4* and *CCT5*, which encode members of the cytosolic chaperonin Cct ring complex that participates in the assembly of tubulin, and *RBL2*, which is involved in microtubule morphogenesis, suggesting a possible microtubule-related role for this paralog pair (*30*) (fig. S5B). The *ecm13*Δ *yjr115w*Δ double mutant was specifically sensitive to benomyl, a microtubule-disrupting agent (fig. S5, C and D), and showed a delay in spindle nucleation and polymerization (fig. S5E). Moreover, the Ecm13 protein interacts with Dad2 and Dad4, which are components of the Dam1 complex that links kinetochores to microtubules to facilitate chromosome segregation (*58*). Consistent with a role in spindle function and chromosome segregation, we found that both GFP-Ecm13 and GFP-Yjr115w showed a distinct nuclear localization (fig. S5F). Another poorly characterized pair is *STB6-STB2*, which encodes proteins that bind the *SIN3* transcriptional repressor and may impinge on the MTC (maintenance of telomere capping) pathway, suggesting a role in aromatic amino acid permease secretion (*30*) (fig. S5, G to J).

Correlation analysis of position-specific evolutionary rate patterns between paralogs

To further explore the factors that drive paralog retention and produce a spectrum of functional redundancy, we considered the relationship among divergent evolution, structure, and function. A negative correlation of trigenic interaction fraction with measures of divergent evolution may be indicative of the constraints that govern this process (Fig. 4B). Amino acid conservation in specific positions indicates evolutionary constraints on amino acid residues that are important for protein function, including those involved in oligomerization, protein-protein interactions, and protein-substrate interactions (*59*). We therefore used the correlation of position-specific evolutionary rate patterns between paralogs as a measure of evolutionary divergence of the sequence constraints (*42*). We reasoned that if both paralogs share constraints on specific residues of protein domains during evolution and evolve similarly after the WGD, then they would be expected to be more similar to each other than to the pre-WGD species. On the other hand, if paralogs do not share constraints on specific residues of protein domains during evolution and evolve differently after the WGD, then they would be less similar to each other than to the pre-WGD species. We therefore designated a set of pairs with a high correlation of position-specific evolutionary rate patterns as evolutionarily constrained pairs for which the correlation of rates between extant sisters was greater than or equal to both the correlations between each sister and the pre-WGD homolog. Paralog pairs with little correlation in their position-specific evolutionary rate patterns have different sequence constraints and are therefore likely to have different structure and function (Fig. 6A and table S12).

For example, the proteins encoded by the *MRS3-MRS4* gene pair show a high correlation in their position-specific evolutionary rate patterns and also have high protein sequence identity (~76%) (Fig. 6B and fig. S6A). Although both *MRS3* and *MRS4* encode high-affinity mitochondrial Fe^{2+} transporters, the *MRS3* protein displays an additional Cu^{2+} transport function (*60*). The general mitochondrial carrier function is structurally constrained because all mitochondrial carrier proteins have a tripartite structure with three similar segments, each of which is ~100 amino acids in length and forms two membrane-spanning α helices (fig. S7A) (*61*). Interestingly, these proteins appear to have properties that are favorable for retention after duplication because multiple mitochondrial carrier protein genes were retained after the yeast WGD. Indeed, of the 35 different mitochondrial carrier protein genes in the yeast genome, 10 are encoded by five WGD paralog pairs (*62*).

Our study interrogated four mitochondrial carrier protein WGD pairs: *MRS3-MRS4*, *YIA6-YEA6*, *YMC1-YMC2*, and *ODC1-ODC2*. Like the *MRS3-MRS4* paralog pair, *YIA6* and *YEA6* are connected by a negative digenic interaction and show a high trigenic interaction fraction, which is consistent with a retained functional

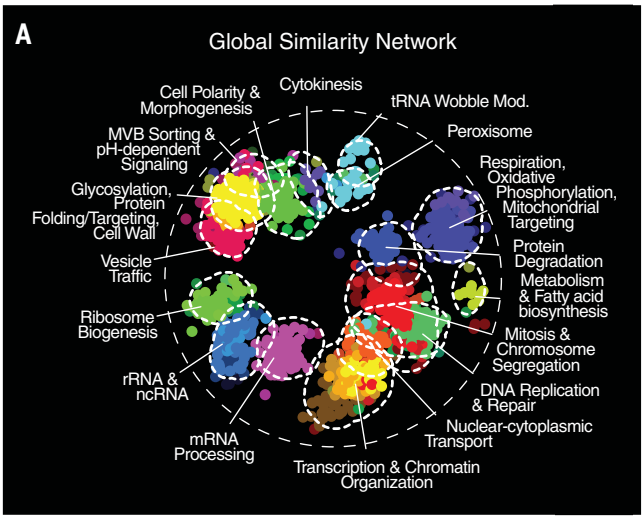

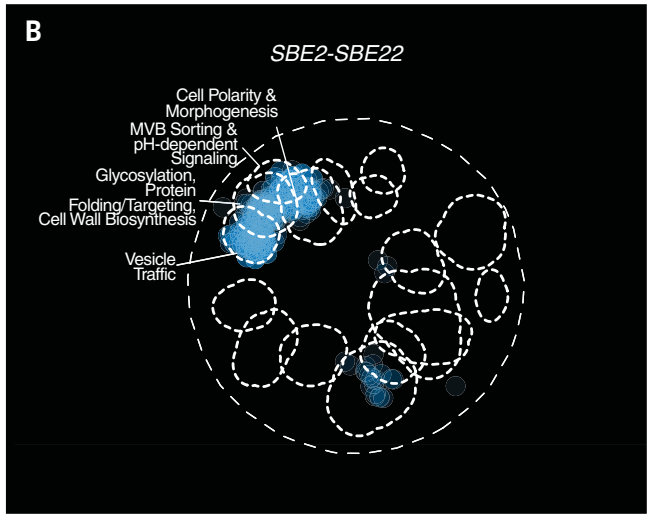

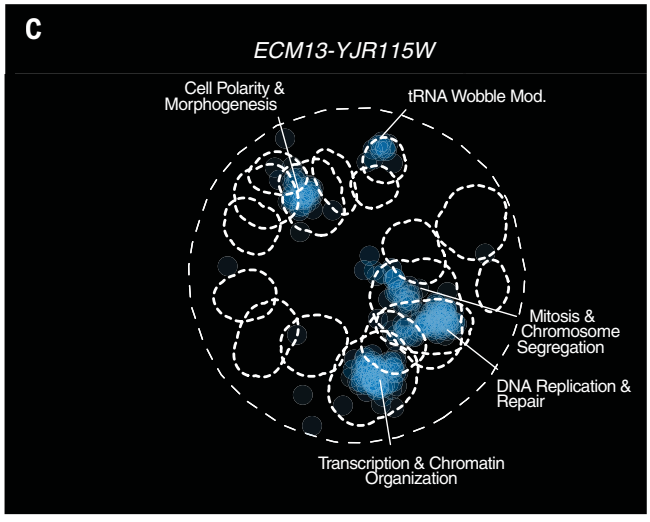

Fig. 5. The trigenic interaction fraction reveals the functional divergence of duplicated genes and illuminates gene function. (**A** to **C**) SAFE (*70*) analysis (A) was used to visualize regions of the global digenic interaction profile similarity network (*30*) that were enriched for genes in the trigenic interaction profiles of the paralog pairs *SBE2-SBE22* (B) and *ECM13-YJR115W* (C). Blue indicates the enrichment related to negative trigenic interactions ($\tau < -0.08$, $P < 0.05$).

redundancy. In contrast, both the *YMC1-YMC2* and *ODC1-ODC2* paralog pairs display relatively few trigenic interactions. Indeed, the *YMC1-YMC2* pair displays a low correlation of position-specific evolutionary rate patterns and thus a low level of functional redundancy (table S12). On the other hand, *ODC1-ODC2* displays a relatively high correlation of position-specific evolutionary rate patterns (table S12); however, their functional overlap may be masked by the presence of other mitochondrial carrier proteins because they belong to a large gene family with multiple paralog members, expanded also by small-scale duplications (table S9). Moreover, we combined our genetic analysis with literature curated data to map a genetic network underlying numerous mitochondrial carrier protein genes, and the *YMC1-YMC2* and *ODC1-ODC2* paralogs appear to form a highly connected subnetwork (fig. S8), which suggests that these two paralog pairs display a more complex functional redundancy.

In contrast to *MRS3-MRS4*, the *SKI7-HBS1* proteins show a relatively low correlation in their position-specific evolutionary rate patterns and thus show a low sequence identity (~26%) with an asymmetric rate of sequence divergence, whereby Ski7 appears to be diverging faster than Hbs1 (table S10). Detailed inspection of these proteins revealed that the Hbs1 protein resembles the pre-WGD homolog, whereas Ski7 has adopted a more divergent fate, which suggests that its evolved role was not constrained structurally by the pre-WGD ancestor (Fig. 6B and fig. S6B). Despite retaining the EF-Tu GTP-binding domain (PF00009), it is present in a highly divergent form. Ski7 also lost critical sequences encoding an Hbs1-like N-terminal motif (PF8938) and sequences encoding the EF-Tu C-terminal domain (PF03143), highlighting the evolutionary divergence of Ski7 from Hsb1 and the pre-WGD homolog (Fig. 6B and fig. S6B).

By calculating the level of correlation of position-specific evolutionary rate patterns between members of the duplicate pair in relation to the pre-WGD homolog (Fig. 6A), we assessed the evolutionary constraints acting on paralogs (Fig. 6C). We found that paralogs with a high trigenic interaction fraction were composed of a significantly higher number of paralogs with correlated evolutionary rate patterns and thus were more evolutionarily constrained than those characterized by a low trigenic interaction fraction (Fisher exact test, $P = 0.01$) (Fig. 6C). Moreover, paralogs that show a synthetic lethal genetic interaction are considered highly functionally redundant. This subset of essential paralogs shows a higher correlation in their position-specific evolutionary rate patterns, which suggests that these genes are more evolutionarily constrained than those within the subset of highly redundant nonessential paralogs displaying a high trigenic interaction fraction (Fisher exact test, $P = 0.02$) (Fig. 6C and table S13). Hence, it appears that some paralogs are highly structurally constrained or "entangled," which limits their divergence leading to the maintenance of functional overlap, but presumably within a context that also enables the evolution of novel functions.

Modeling simulates the divergent evolution of paralogs with retained functional redundancy

We also explored functional redundancy and paralog retention using in silico modeling in an attempt to test two hypotheses. Under the first hypothesis, the retained nonessential paralog pairs with a high trigenic interaction fraction—and thus a high functional overlap—are inherently unstable over evolutionary time and would eventually diverge completely, losing any common functionality. Under the alternative hypothesis, retained paralogs may converge to an evolutionary steady state, in which paralogs with retained functional overlap cannot segregate certain functional regions without a fitness cost. We computationally generated "genes" of fixed length, in which regions of random length were assigned responsibility for a function, and a random number of such functions was generated for each gene, such that these functional regions were allowed to overlap. Then we duplicated each gene and began introducing random "degenerative" mutations, which would render the affected paralog unable to perform any function associated with the mutated region (Fig. 7A). We discarded any lineage as unfit when any one of the original functions could not be carried out by at least one sister, and continued simulating mutations until the pair reached steady state and could tolerate no additional mutations. The extent of overlap of functions in each randomly generated ancestral gene at the start of paralog evolution provides a measure of their initial structural and functional "entanglement," generating a baseline from which we assessed their evolutionary trajectories (*42*).

These simulations revealed that for a large fraction of paralog pairs, the mutation process resulted in a singleton state with only one of the sisters being retained. A sizable fraction of

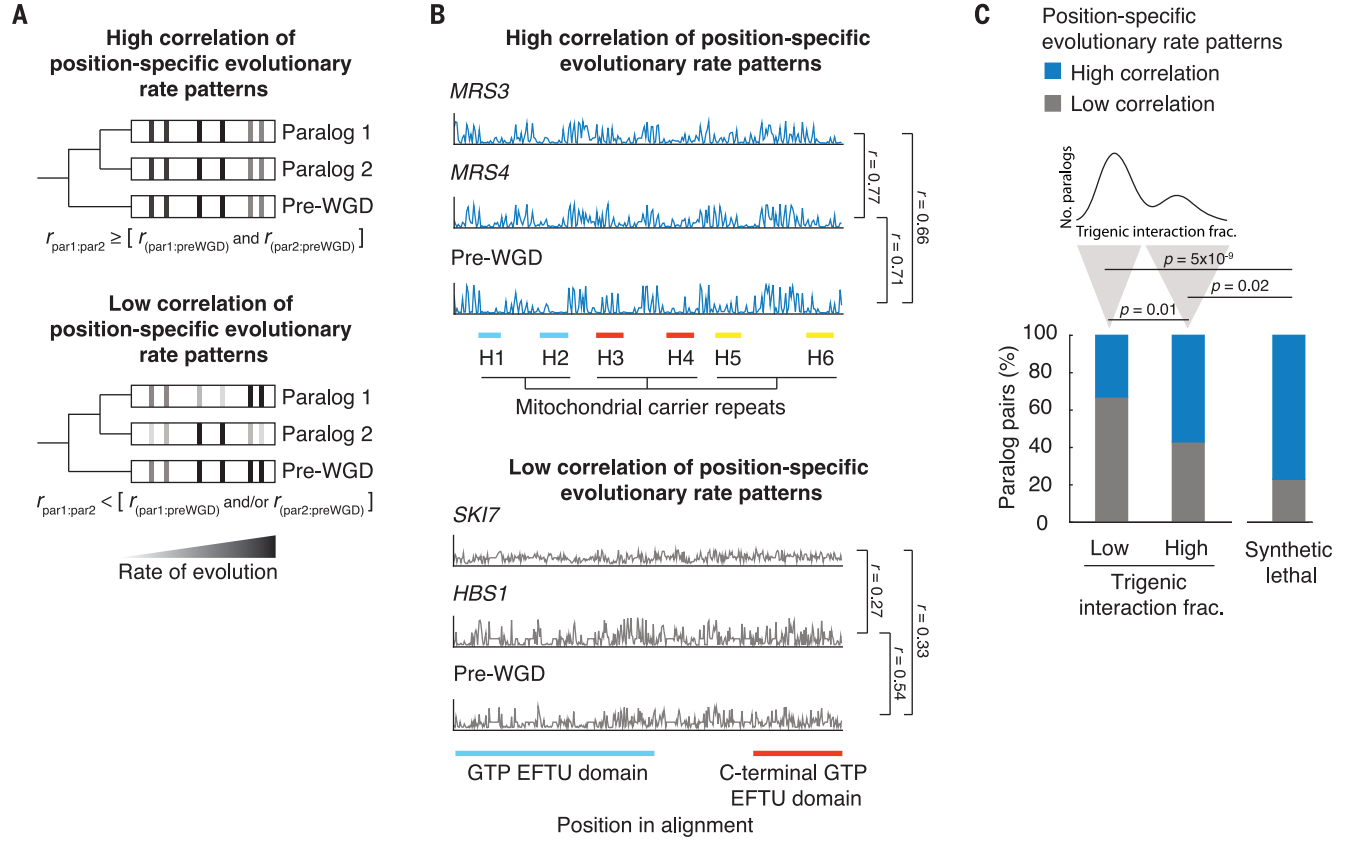

Fig. 6. Evolution of retained overlap due to evolutionary constraints acting on duplicated gene sequences. (**A**) Schematic depiction of the analysis of correlated evolutionary sequence changes across paralog sequences reflecting evolutionary constraints on paralogs. Correlated rates of evolution for specific columns in multiple sequence alignments for the pre-WGD homolog and each paralog are denoted with a gray-to-black gradient, from low to high, respectively. High correlation of position-specific evolutionary rate patterns identifies residues with similar evolutionary constraints. Paralogs with correlated rates ($r_{par1:par2}$) that are greater than or equal to that of each paralog and with the corresponding pre-WGD ($r_{par1:preWGD}$ and $r_{par2:preWGD}$) were designated as having a high correlation of position-specific evolutionary rate pattern, and paralogs with correlated rates ($r_{par1:par2}$) that were less than that of either paralog or both paralogs with the pre-WGD ($r_{par1:preWGD}$ and/or $r_{par2:preWGD}$) were designated as having a low correlation of position-specific evolutionary rate pattern; *r* refers to the Pearson correlation coefficient between the respective sequences. (**B**) Examples of evolutionary rates for positions in the alignments for representative paralogs, showing a high correlation of position-specific evolutionary rate patterns (*MRS3-MRS4*) or a low correlation of position-specific evolutionary rate patterns (*SKI7-HBS1*). The position in the alignment is plotted on the *x* axis; the rate of evolution at a particular position divided by the average rate of evolution for all residues in the given sister paralog is plotted on the *y* axis. The scale of the *y* axis has been fixed for each paralog pair. Pfam domains are annotated. The *MRS3-MRS4* alignment shows three mitochondrial carrier repeats, each composed of two α helices (blue, H1 and H2; red, H3 and H4; yellow, H5 and H6) followed by a characteristic motif Pro-X-[Asp/Glu]-X-X-[Lys/Arg]-X-[Lys/Arg]-(20 to 30 residues)-[Asp/Glu]-Gly-X-X-X-X-[Trp/Tyr/Phe]-[Lys/Arg]-Gly connecting each pair of membrane-spanning domains by a loop. The *SKI7-HBS1* alignment shows GTP EF-Tu (blue) and C-terminal GTP EF-Tu (red) domains. The Hbs1-like N-terminal motif lies outside of the alignment window. (**C**) Fraction of nonessential and essential paralogs that show a high or low correlation of position-specific evolutionary rate patterns. The paralogs with low and high trigenic interaction fraction belong to the part of the distribution shown above; a trigenic interaction fraction cutoff of 0.4 was used, based on negative interactions (τ or ε) < −0.08, $P < 0.05$, and contains the set of paralogs that were used for the correlated evolution analysis. Significance was assessed by Fisher exact test.

simulations, however, ended with paralogs in a stable steady state in which no more mutations could be tolerated in either paralog, while still maintaining viability. Analysis of the simulation results revealed that the particular trajectory followed by a given paralog pair was correlated with the level of functional entanglement. Specifically, paralog pairs that started with the highest levels of entanglement immediately upon duplication were more likely to revert to a singleton state. This suggests that duplicated genes generally cannot tolerate genetic perturbations when they lack functionally independent regions (Fig. 7B and fig. S9A). Among paralog pairs that were retained at steady state, increased entanglement at the point of duplication also led to a broader bias in the functional asymmetry (ratio of functional responsibilities) at steady state. Thus, paralogs diverge asymmetrically when they begin their evolutionary trajectory with a protein sequence containing extensive entanglement (Fig. 7C and fig. S9, B and C). Consistent with this observation from our simulations, paralog evolution can show asymmetric bias with respect to functional redundancy (Fig. 4B).

Our modeling further revealed that as the extent of the initial entanglement of paralogs increased, so did the range of steady-state functional overlap, which is represented by constrained domains at steady state (Fig. 7D and fig. S9D). This suggests that the bimodal distribution of the trigenic interaction fraction (Fig. 4A) may indicate that one subset of WGD paralogs diverged substantially so that each of the sister paralogs has a distinct function, and another subset of retained WGD paralogs reached an evolutionary steady state despite retained functional overlap, perhaps as a result of their structural and functional entanglement (Fig. 7E). For example, in the case of *SKI7-HBS1*, Ski7 diverged from Hbs1 by losing the Hbs1-like N-terminal motif and the EF-Tu C-terminal domain while retaining a highly diverged form of the EF-Tu GTP-binding domain, reflecting a modular, structural, and functional organization of the protein (Fig. 6B). On the other hand, *MRS3* and *MRS4* encode mitochondrial carrier proteins dedicated to the transport of small inorganic ions, and thus their divergence would be predicted to occur in specific residues that modulate ion specificity (Fig. 6B and fig. S7).

We propose that the evolutionary fate of a duplicated gene can be governed by an interplay of structural and functional entanglement (Fig. 7E). If a duplicated gene contains several easily partitioned functions, then it will most likely subfunctionalize; on the other hand, an entangled pair, which is highly restricted structurally and functionally, would have a tendency to revert to a singleton state because one of the genes is predicted to quickly become nonfunctional. However, given multiple functions and an

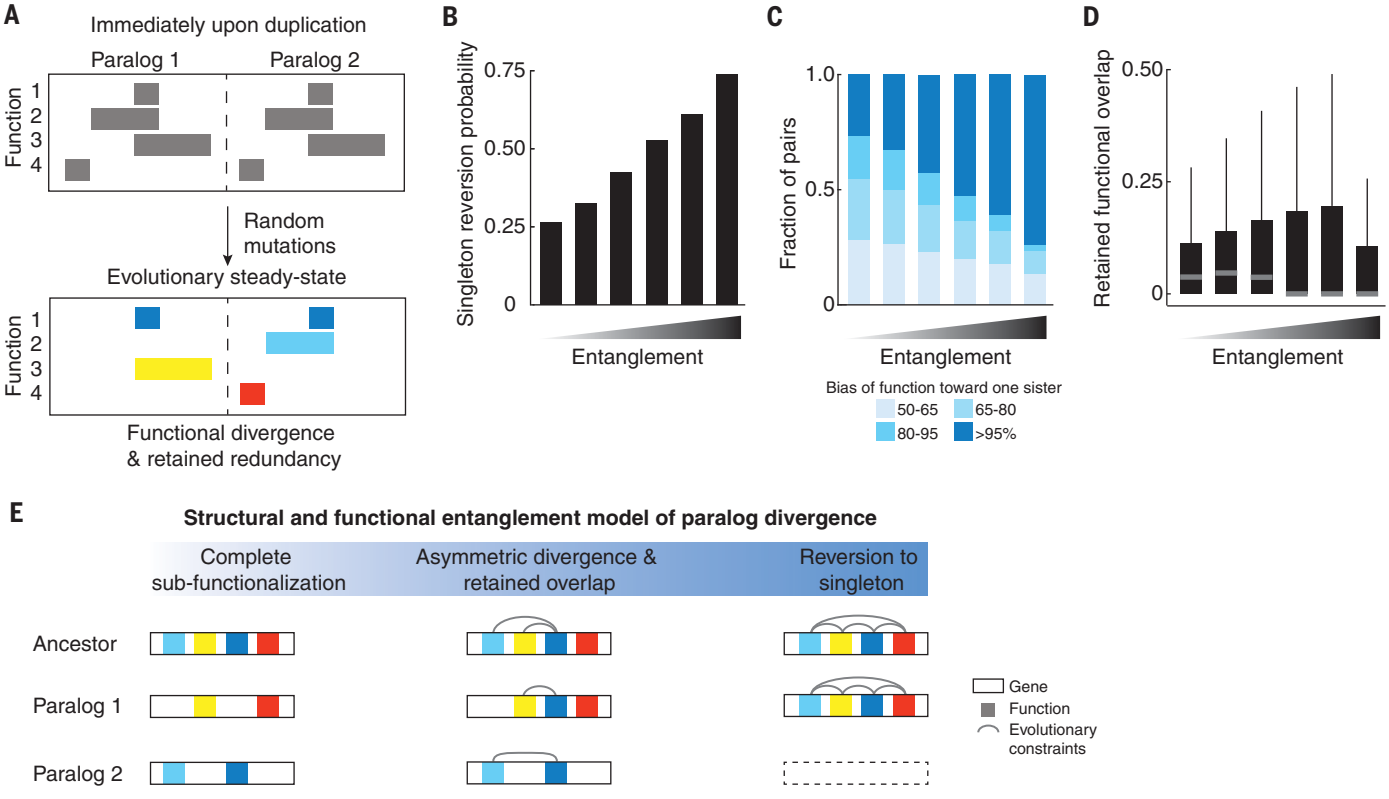

Fig. 7. In silico evolutionary model. (**A**) Schematic depiction of the in silico evolutionary model. The pair evolves through random mutations until it reaches an evolutionarily stable state that can sustain no further mutations without a loss of function. Top, a pair at the start of the evolutionary trajectory; bottom, a pair that achieves a division of labor with a retention of a common function (dark blue blocks), the loss of which is prevented because it would compromise the unique functions of each paralog (yellow, light blue, red). (**B** to **D**) Evolutionary fates of paralogs with functional and structural entanglement. Paralogs were generated to represent a range of overlapping functional domains at the onset of their evolutionary trajectory, and the propensity to assume specific paralog properties was quantified. In each case, the *x* axis represents bins of initial functional overlap as a fraction of "gene" length at the start of the simulations (< 10%, 30%, 50%, 70%, 90%, 100%, respectively); the *y* axis depicts the propensities of paralogs to revert to a singleton state (B), evolve functional asymmetry (C), or retain functional overlap at the evolutionary steady state (D). (**E**) The structural and functional entanglement model of paralog divergence. A pair will evolve by subfunctionalization if it is modular and is composed of partitionable functions (left). A paralog pair that is very structurally and functionally entangled will have a high probability of reversion to a singleton state because one of the sisters will quickly degenerate (right). Paralogs with an intermediate level of entanglement at the time of duplication will tend to partition some and retain some overlapping functions, allowing for specialization of a common activity (center).

intermediate level of entanglement, a gene pair has a chance of partitioning or expanding some nonoverlapping functions while retaining others in common, and remaining evolutionarily stable.

Discussion

The complex genetic interaction network of dispensable WGD paralogs provides insight into the long-standing question of why paralogs with overlapping functions are retained on an evolutionary time scale. By combining both paralog-specific digenic interactions and the paralog pair trigenic interactions in a single metric, the trigenic interaction fraction, we captured the spectrum of the retained functional redundancy of dispensable paralogs.

Definitions of functionally redundant or divergent paralogs using genetic interactions appear to be consistent with classification from protein-protein interaction studies (*25*). For example, in the case where a paralog is deleted and the sister responds by gaining specific protein-protein interactions, then the paralogs should compensate for each other's loss and thus should exhibit a high trigenic interaction fraction. Indeed, four such paralogs were examined in our study and they showed a propensity to exhibit high trigenic interaction fractions. In particular, *NUP53-ASM4* and *OSH6-OSH7* showed high trigenic interaction fractions of 0.49 and 0.80, respectively. On the other hand, some paralogs share protein-protein interactions that are lost for both paralogs when only one sister is deleted, which suggests that although these paralogs may cooperate, they do not fully compensate for each other (*25*). We examined two such known paralogs, *PEX25-PEX27* and *GSY1-GSY2*, and they exhibited low trigenic interaction fractions of 0.19 and 0.25, respectively. Beyond these examples, genetic interaction profiling provides a functional readout and allows assessment of pairs of genes that do not have extensive protein-protein interaction profiles, and therefore it provides a complementary view of functional redundancy.

Our framework enabled us to interrogate how WGD paralog evolution relates to the evolutionary stability of retained common functions and asymmetric functional divergence. By computing the extent of correlated evolution in sister paralogs (Fig. 6), we identified paralogs that show highly correlated position-specific evolutionary rate patterns and thus are under strong evolutionary constraints to retain some of their ancestral function, reflecting their structural and functional entanglement. This was further explored by our in silico model (Fig. 7), which predicts that low levels of entanglement are sufficient to drive asymmetric subfunctionalization, whereas more complex sequence-function relationships with higher structural entanglement can result in fixation of functional redundancy. Indeed, our modeling shows that given some level of moderate structural entanglement and the potential for multifunctionality, a substantial fraction of duplicate pairs converge to a steady state in which they retain functional overlap. This result offers a possible explanation as to the persistence of the functional overlap in paralogs, which is not simply due to paralogs diverging slowly from one another. We propose that the results of our in silico modeling may explain why the trigenic interaction fraction tends to follow a bimodal distribution (Figs. 4A and 7). The upper mode of the distribution represents the set of duplicate pairs that will likely remain fixed in a partially functionally redundant state, whereas the lower mode represents duplicates that already have or are diverging in function. Because ohnologs and homeologs (*42*, *50*) show the same distribution of trigenic interaction fraction, this model of paralog divergence and retention of functional redundancy also likely applies to gene duplicates of various ages and origins beyond WGD, which may include small-scale duplicates.

In the simulation analysis, we modeled functions as being supported by contiguous sequence domains. However, because our model treats every position along a "gene" as statistically independent, positions contributing to a common function would not need to be contiguous, and the conclusions would remain the same for functional domains encoded by discontinuous sequences. Therefore, the model has the flexibility to capture a wide variety of different physiological scenarios that might display structural or functional entanglement, such as independent modular domains; linearly distant contact sites within a secondary, tertiary, or quaternary structure; or even regulatory regions beyond coding boundaries or elsewhere within the genome. It is important to note that this definition of structural and functional entanglement is distinct from the simple physical entanglement of proteins restricted to the basic organization of polypeptide chains (*63*).

The question of why subfunctionalization does not proceed to completion—leading to fixation of duplicated genes with some specific functions, yet exhibiting a certain level of functional redundancy—remains an outstanding problem in evolutionary biology. Constraints that prevent complete divergence may allow paralogs to retain the ability to function in parallel biochemical pathways or macromolecular complexes, thus resulting in a retention of redundancy (*18*, *43*, *64*). More specifically, despite functional divergence of independent domains, incomplete subfunctionalization of paralogs could be driven by a structurally and functionally overlapping ancestral domain (*35*). There are few existing models of duplicate evolution that specifically address the existence of redundancy in a steady state. There are models that address different potential modes of functional divergence, such as neo- or subfunctionalization (*39*, *65*). However, reasons for the persistence of functional redundancy have remained elusive. It is noteworthy that previous simple computer simulations, which incorporated mutation rates of genes and the varying contribution of their functions to overall fitness, have also identified situations in which redundancy can be maintained indefinitely (*66*–*68*). It has been shown that paralogs that are selected to function as distinct homomers also retain the ability to heterodimerize, which may prevent functional divergence between paralogs (*69*). In general, our findings support fixation of overlapping functional redundancy for a substantial proportion of yeast paralogs.

Methods summary

To study the functional divergence of duplicated genes, 240 double mutants and 480 corresponding single mutant control "query" strains, involving dispensable WGD pairs in the budding yeast *Saccharomyces cerevisiae* S288C, were constructed using PCR-mediated gene deletion followed by tetrad analysis. Paralog 1 deletion was marked with *natMX4*, while paralog 2 was deleted and replaced with *K. lactis URA3*. Single mutant control strains deleted for each one of the paralogs were also marked with the relevant control marker, which was inserted at the benign *HO* locus. Query strain fitness and query gene pair genetic interactions were measured using high-density synthetic genetic array (SGA) analysis. To obtain trigenic interactions, double mutant query strains along with their respective single mutant control query strains were subjected to trigenic-SGA analysis (τ-SGA), which involves a number of automated replica pinning steps. Each query strain was mated to a diagnostic array of 1200 strains, consisting of deletion mutants of nonessential genes and temperature-sensitive alleles of essential genes, providing a representative view of the global digenic interaction network. Briefly, the query and array strains were mated on rich media, *MAT***a**/α diploids were selected on media containing G418 and clonNAT, sporulation was induced by transferring to media with low levels of nitrogen and carbon sources, and *MAT***a** meiotic haploid progeny was selected on haploid selection media. Triple mutants were then selected by first pinning onto haploid selection media containing G418, lacking uracil, and then onto haploid selection media containing both G418 and clonNAT, lacking uracil. Every query strain was screened in two independent replicates.

Colony size was measured as a proxy for fitness, and digenic and trigenic interactions were scored using a quantitative model. Trigenic

interactions were classified into novel versus modified by overlapping with digenic interactions. Functional information embedded within digenic and trigenic interactions was assessed by their enrichment with external functional standards, such as protein-protein interactions, subcellular localization, coexpression, and co-annotation. Trigenic interaction fraction was calculated as the ratio of the negative trigenic interaction degree relative to the total negative digenic and trigenic interaction degree. Correlation of trigenic interaction fraction with physiological and evolutionary features included quantification of genetic interactions within a paralog pair, asymmetry of digenic interactions of members of each paralog pair, and sequence divergence rate, which was calculated as the raw difference between the fold-changes in substitutions per site in post-WGD clades. The potential for paralog induction during developmental programs was assessed in (i) meiosis using published meiotic mRNA-seq and ribosome profiling datasets, (ii) filamentous growth using a published measure of invasion, as well as (iii) glucose starvation conditions using published gene expression dataset. Dosage selection was estimated using global digenic interaction profile correlation similarity.

SAFE (Functional annotations based on the Spatial Analysis of Functional Enrichment) of the global genetic interaction profile similarity network was used to annotate gene function. Enrichment was calculated using the overlap of trigenic interactions with a neighborhood on the global digenic interaction similarity network. Novel paralog function for *ECM13-YJR115W* was interrogated using a drug sensitivity spot assay on media containing benomyl, and a liquid growth curve analysis on media containing latrunculin B. Spindle morphology was monitored by expressing Tub1-GFP, as well as sfGFP fusion proteins of Ecm13 and Yjr115w and imaging the resulting strains using a spinning-disc confocal microscope. Novel paralog function for *STB2-STB6* was monitored by Bap2-GFP localization in *stb2*Δ *stb6*Δ double mutant deletion strains and quantified using CellProfiler.

To measure evolutionary constraints on paralogs, evolutionary rates for specific amino acid columns in multiple sequence alignments were computed using the discrete gamma model of protein evolution, as implemented in PAML for the pre-WGD sequences and for each paralog separately. Pearson correlation coefficients were computed between the rates of the pre-WGD clade to each paralog (pre-WGD & Paralog 1 and pre-WGD and Paralog 2), and between the two paralogs (Paralog 1 and Paralog 2) to classify paralogs into those with low and high correlation of position specific evolutionary rate patterns. BioGRID was used to curate genetic interactions for the mitochondrial carrier protein family. Paralog divergence was simulated using a computational framework in which a gene of fixed length was generated, annotated with hypothetical functions and subjected to random degenerative mutations at a constant rate. Evolution to a steady state was achieved when no more divergence mutations could be tolerated while maintaining viability. The resulting paralogs were binned according to each pair's initial level of structural entanglement, which is the level of mutable positions within a gene that carry out two or more functions to quantify the number of paralogs that reverted to singleton state, completely diverged or retained functional overlap. For a more detailed description of the experimental and computational analyses, refer to the supplementary materials.

REFERENCES AND NOTES

1. J. E. Bowers, B. A. Chapman, J. Rong, A. H. Paterson, Unravelling angiosperm genome evolution by phylogenetic analysis of chromosomal duplication events. *Nature* **422**, 433–438 (2003). doi: 10.1038/nature01521; pmid: 12660784
2. P. Dehal, J. L. Boore, Two rounds of whole genome duplication in the ancestral vertebrate. *PLOS Biol.* **3**, e314 (2005). doi: 10.1371/journal.pbio.0030314; pmid: 16128622
3. Y. Guan, M. J. Dunham, O. G. Troyanskaya, Functional analysis of gene duplications in Saccharomyces cerevisiae. *Genetics* **175**, 933–943 (2007). doi: 10.1534/genetics.106.064329; pmid: 17151249
4. S. Maere *et al*., Modeling gene and genome duplications in eukaryotes. *Proc. Natl. Acad. Sci. U.S.A.* **102**, 5454–5459 (2005). doi: 10.1073/pnas.0501102102; pmid: 15800040
5. E. E. Eichler, Recent duplication, domain accretion and the dynamic mutation of the human genome. *Trends Genet.* **17**, 661–669 (2001). doi: 10.1016/S0168-9525(01)02492-1; pmid: 11672867
6. M. Kellis, B. W. Birren, E. S. Lander, Proof and evolutionary analysis of ancient genome duplication in the yeast Saccharomyces cerevisiae. *Nature* **428**, 617–624 (2004). doi: 10.1038/nature02424; pmid: 15004568
7. K. H. Wolfe, D. C. Shields, Molecular evidence for an ancient duplication of the entire yeast genome. *Nature* **387**, 708–713 (1997). doi: 10.1038/42711; pmid: 9192896
8. J. Thornton, in *Evolutionary Genetics: Concepts and Case Studies*, C. W. Fox, J. B. Wolf, Eds. (Oxford Univ. Press, New York, 2006), pp. 160–161.
9. S. Ohno, in *Evolution by Gene Duplication* (Springer, 1970), chap. 10, p. 59.
10. I. Wapinski, A. Pfeffer, N. Friedman, A. Regev, Natural history and evolutionary principles of gene duplication in fungi. *Nature* **449**, 54–61 (2007). doi: 10.1038/nature06107; pmid: 17805289
11. C. Seoighe, K. H. Wolfe, Yeast genome evolution in the post-genome era. *Curr. Opin. Microbiol.* **2**, 548–554 (1999). doi: 10.1016/S1369-5274(99)00015-6; pmid: 10508730
12. K. P. Byrne, K. H. Wolfe, The Yeast Gene Order Browser: Combining curated homology and syntenic context reveals gene fate in polyploid species. *Genome Res.* **15**, 1456–1461 (2005). doi: 10.1101/gr.3672305; pmid: 16169922
13. Z. Gu *et al*., Role of duplicate genes in genetic robustness against null mutations. *Nature* **421**, 63–66 (2003). doi: 10.1038/nature01198; pmid: 12511954
14. L. Grassi *et al*., Identity and divergence of protein domain architectures after the yeast whole-genome duplication event. *Mol. Biosyst.* **6**, 2305–2315 (2010). doi: 10.1039/c003507f; pmid: 20820472
15. A. Baudot, B. Jacq, C. Brun, A scale of functional divergence for yeast duplicated genes revealed from analysis of the protein-protein interaction network. *Genome Biol.* **5**, R76 (2004). doi: 10.1186/gb-2004-5-10-r76; pmid: 15461795
16. L. Hakes, J. W. Pinney, S. C. Lovell, S. G. Oliver, D. L. Robertson, All duplicates are not equal: The difference between small-scale and genome duplication. *Genome Biol.* **8**, R209 (2007). doi: 10.1186/gb-2007-8-10-r209; pmid: 17916239
17. J. Li, Z. Yuan, Z. Zhang, The cellular robustness by genetic redundancy in budding yeast. *PLOS Genet.* **6**, e1001187 (2010). doi: 10.1371/journal.pgen.1001187; pmid: 21079672
18. B. Papp, C. Pál, L. D. Hurst, Metabolic network analysis of the causes and evolution of enzyme dispensability in yeast. *Nature* **429**, 661–664 (2004). doi: 10.1038/nature02636; pmid: 15190353
19. D. Vitkup, P. Kharchenko, A. Wagner, Influence of metabolic network structure and function on enzyme evolution. *Genome Biol.* **7**, R39 (2006). doi: 10.1186/gb-2006-7-5-r39; pmid: 16684370
20. R. Kafri, A. Bar-Even, Y. Pilpel, Transcription control reprogramming in genetic backup circuits. *Nat. Genet.* **37**, 295–299 (2005). doi: 10.1038/ng1523; pmid: 15723064
21. X. Gu, Z. Zhang, W. Huang, Rapid evolution of expression and regulatory divergences after yeast gene duplication. *Proc. Natl. Acad. Sci. U.S.A.* **102**, 707–712 (2005). doi: 10.1073/pnas.0409186102; pmid: 15647348
22. G. C. Conant, K. H. Wolfe, Functional partitioning of yeast co-expression networks after genome duplication. *PLOS Biol.* **4**, e109 (2006). doi: 10.1371/journal.pbio.0040109; pmid: 16555924
23. I. Tirosh, N. Barkai, Comparative analysis indicates regulatory neofunctionalization of yeast duplicates. *Genome Biol.* **8**, R50 (2007). doi: 10.1186/gb-2007-8-4-r50; pmid: 17411427
24. A. DeLuna, M. Springer, M. W. Kirschner, R. Kishony, Need-based up-regulation of protein levels in response to deletion of their duplicate genes. *PLOS Biol.* **8**, e1000347 (2010). doi: 10.1371/journal.pbio.1000347; pmid: 20361019
25. G. Diss *et al*., Gene duplication can impart fragility, not robustness, in the yeast protein interaction network. *Science* **355**, 630–634 (2017). doi: 10.1126/science.aai7685; pmid: 28183979
26. R. Mani, R. P. St. Onge, J. L. Hartman 4th, G. Giaever, F. P. Roth, Defining genetic interaction. *Proc. Natl. Acad. Sci. U.S.A.* **105**, 3461–3466 (2008). doi: 10.1073/pnas.0712255105; pmid: 18305163
27. P. Novick, D. Botstein, Phenotypic analysis of temperature-sensitive yeast actin mutants. *Cell* **40**, 405–416 (1985). doi: 10.1016/0092-8674(85)90154-0; pmid: 3967297
28. A. Bender, J. R. Pringle, Use of a screen for synthetic lethal and multicopy suppressee mutants to identify two new genes involved in morphogenesis in Saccharomyces cerevisiae. *Mol. Cell. Biol.* **11**, 1295–1305 (1991). doi: 10.1128/MCB.11.3.1295; pmid: 1996092
29. J. van Leeuwen *et al*., Exploring genetic suppression interactions on a global scale. *Science* **354**, aag0839 (2016). doi: 10.1126/science.aag0839; pmid: 27811238
30. M. Costanzo *et al*., A global genetic interaction network maps a wiring diagram of cellular function. *Science* **353**, aaf1420 (2016). doi: 10.1126/science.aaf1420; pmid: 27708008
31. A. H. Tong *et al*., Global mapping of the yeast genetic interaction network. *Science* **303**, 808–813 (2004). doi: 10.1126/science.1091317; pmid: 14764870
32. M. Costanzo *et al*., The genetic landscape of a cell. *Science* **327**, 425–431 (2010). doi: 10.1126/science.1180823; pmid: 20093466
33. B. VanderSluis *et al*., Genetic interactions reveal the evolutionary trajectories of duplicate genes. *Mol. Syst. Biol.* **6**, 429 (2010). doi: 10.1038/msb.2010.82; pmid: 21081923
34. G. Musso *et al*., The extensive and condition-dependent nature of epistasis among whole-genome duplicates in yeast. *Genome Res.* **18**, 1092–1099 (2008). doi: 10.1101/gr.076174.108; pmid: 18463300
35. E. J. Dean, J. C. Davis, R. W. Davis, D. A. Petrov, Pervasive and persistent redundancy among duplicated genes in yeast. *PLOS Genet.* **4**, e1000113 (2008). doi: 10.1371/journal.pgen.1000113; pmid: 18604285
36. A. DeLuna *et al*., Exposing the fitness contribution of duplicated genes. *Nat. Genet.* **40**, 676–681 (2008). doi: 10.1038/ng.123; pmid: 18408719
37. E. Kuzmin *et al*., Systematic analysis of complex genetic interactions. *Science* **360**, eaao1729 (2018). doi: 10.1126/science.aao1729; pmid: 29674565
38. J. Ihmels, S. R. Collins, M. Schuldiner, N. J. Krogan, J. S. Weissman, Backup without redundancy: Genetic interactions reveal the cost of duplicate gene loss. *Mol. Syst. Biol.* **3**, 86 (2007). doi: 10.1038/msb4100127; pmid: 17389874
39. A. Force *et al*., Preservation of duplicate genes by complementary, degenerative mutations. *Genetics* **151**, 1531–1545 (1999). pmid: 10101175
40. A. van Hoof, Conserved functions of yeast genes support the duplication, degeneration and complementation model for gene duplication. *Genetics* **171**, 1455–1461 (2005). doi: 10.1534/genetics.105.044057; pmid: 15965245
41. A. C. Marques, N. Vinckenbosch, D. Brawand, H. Kaessmann, Functional diversification of duplicate genes through

subcellular adaptation of encoded proteins. *Genome Biol.* **9**, R54 (2008). doi: 10.1186/gb-2008-9-3-r54; pmid: 18336717
42. See supplementary materials.
43. A. N. Marshall, M. C. Montealegre, C. Jiménez-López, M. C. Lorenz, A. van Hoof, Alternative splicing and subfunctionalization generates functional diversity in fungal proteomes. *PLOS Genet.* **9**, e1003376 (2013). doi: 10.1371/journal.pgen.1003376; pmid: 23516382
44. A. van Hoof, P. A. Frischmeyer, H. C. Dietz, R. Parker, Exosome-mediated recognition and degradation of mRNAs lacking a termination codon. *Science* **295**, 2262–2264 (2002). doi: 10.1126/science.1067272; pmid: 11910110
45. M. K. Doma, R. Parker, Endonucleolytic cleavage of eukaryotic mRNAs with stalls in translation elongation. *Nature* **440**, 561–564 (2006). doi: 10.1038/nature04530; pmid: 16554824
46. E. R. Kunji, The role and structure of mitochondrial carriers. *FEBS Lett.* **564**, 239–244 (2004). doi: 10.1016/S0014-5793(04)00242-X; pmid: 15111103
47. E. M. Froschauer, R. J. Schweyen, G. Wiesenberger, The yeast mitochondrial carrier proteins Mrs3p/Mrs4p mediate iron transport across the inner mitochondrial membrane. *Biochim. Biophys. Acta* **1788**, 1044–1050 (2009). doi: 10.1016/j.bbamem.2009.03.004; pmid: 19285482
48. G. C. Shaw *et al.*, Mitoferrin is essential for erythroid iron assimilation. *Nature* **440**, 96–100 (2006). doi: 10.1038/nature04512; pmid: 16511496
49. G. G. Perrone, S. X. Tan, I. W. Dawes, Reactive oxygen species and yeast apoptosis. *Biochim. Biophys. Acta* **1783**, 1354–1368 (2008). doi: 10.1016/j.bbamcr.2008.01.023; pmid: 18298957
50. M. Marcet-Houben, T. Gabaldón, Beyond the Whole-Genome Duplication: Phylogenetic Evidence for an Ancient Interspecies Hybridization in the Baker's Yeast Lineage. *PLOS Biol.* **13**, e1002220 (2015). doi: 10.1371/journal.pbio.1002220; pmid: 26252497
51. Z. Cheng *et al.*, Pervasive, Coordinated Protein-Level Changes Driven by Transcript Isoform Switching during Meiosis. *Cell* **172**, 910–923. e16 (2018). doi: 10.1016/j.cell.2018.01.035; pmid: 29474919
52. O. Ryan *et al.*, Global gene deletion analysis exploring yeast filamentous growth. *Science* **337**, 1353–1356 (2012). doi: 10.1126/science.1224339; pmid: 22984072
53. P. H. Bradley, M. J. Brauer, J. D. Rabinowitz, O. G. Troyanskaya, Coordinated concentration changes of transcripts and metabolites in Saccharomyces cerevisiae. *PLOS Comput. Biol.* **5**, e1000270 (2009). doi: 10.1371/journal.pcbi.1000270; pmid: 19180179
54. F. A. Kondrashov, A. S. Kondrashov, Role of selection in fixation of gene duplications. *J. Theor. Biol.* **239**, 141–151 (2006). doi: 10.1016/j.jtbi.2005.08.033; pmid: 16242725
55. A. N. Nguyen Ba *et al.*, Detecting functional divergence after gene duplication through evolutionary changes in posttranslational regulatory sequences. *PLOS Comput. Biol.* **10**, e1003977 (2014). doi: 10.1371/journal.pcbi.1003977; pmid: 25474245
56. W. Qian, J. Zhang, Protein subcellular relocalization in the evolution of yeast singleton and duplicate genes. *Genome Biol. Evol.* **1**, 198–204 (2009). doi: 10.1093/gbe/evp021; pmid: 20333190
57. B. Santos, M. Snyder, Sbe2p and sbe22p, two homologous Golgi proteins involved in yeast cell wall formation. *Mol. Biol. Cell* **11**, 435–452 (2000). doi: 10.1091/mbc.11.2.435; pmid: 10679005
58. S. Westermann *et al.*, Formation of a dynamic kinetochore-microtubule interface through assembly of the Dam1 ring complex. *Mol. Cell* **17**, 277–290 (2005). doi: 10.1016/j.molcel.2004.12.019; pmid: 15664196
59. A. N. Nguyen Ba *et al.*, Proteome-wide discovery of evolutionary conserved sequences in disordered regions. *Sci. Signal.* **5**, rs1 (2012). doi: 10.1126/scisignal.2002515; pmid: 22416277
60. K. E. Vest *et al.*, Overlap of copper and iron uptake systems in mitochondria in Saccharomyces cerevisiae. *Open Biol.* **6**, 150223 (2016). doi: 10.1098/rsob.150223; pmid: 26763345
61. F. Palmieri, C. L. Pierri, A. De Grassi, A. Nunes-Nesi, A. R. Fernie, Evolution, structure and function of mitochondrial carriers: A review with new insights. *Plant J.* **66**, 161–181 (2011). doi: 10.1111/j.1365-313X.2011.04516.x; pmid: 21443630
62. R. Belenkiy, A. Haefele, M. B. Eisen, H. Wohlrab, The yeast mitochondrial transport proteins: New sequences and consensus residues, lack of direct relation between consensus residues and transmembrane helices, expression patterns of the transport protein genes, and protein-protein interactions with other proteins. *Biochim. Biophys. Acta* **1467**, 207–218 (2000). doi: 10.1016/S0005-2736(00)00222-4; pmid: 10930523
63. Y. Zhao, M. Cieplak, Stability of structurally entangled protein dimers. *Proteins* **86**, 945–955 (2018). doi: 10.1002/prot.25526; pmid: 29790597
64. B. Papp, C. Pál, L. D. Hurst, Dosage sensitivity and the evolution of gene families in yeast. *Nature* **424**, 194–197 (2003). doi: 10.1038/nature01771; pmid: 12853957
65. S. Ohno, in *Evolution by Gene Duplication* (Springer, 1970), chap. 13, pp. 71–72.
66. M. A. Nowak, M. C. Boerlijst, J. Cooke, J. M. Smith, Evolution of genetic redundancy. *Nature* **388**, 167–171 (1997). doi: 10.1038/40618; pmid: 9217155
67. A. Wagner, The role of population size, pleiotropy and fitness effects of mutations in the evolution of overlapping gene functions. *Genetics* **154**, 1389–1401 (2000). pmid: 10757778
68. T. Vavouri, J. I. Semple, B. Lehner, Widespread conservation of genetic redundancy during a billion years of eukaryotic evolution. *Trends Genet.* **24**, 485–488 (2008). doi: 10.1016/j.tig.2008.08.005; pmid: 18786741
69. A. Marchant *et al.*, The role of structural pleiotropy and regulatory evolution in the retention of heteromers of paralogs. *eLife* **8**, e46754 (2019). doi: 10.7554/eLife.46754; pmid: 31454312
70. A. Baryshnikova, Systematic Functional Annotation and Visualization of Biological Networks. *Cell Syst.* **2**, 412–421 (2016). doi: 10.1016/j.cels.2016.04.014; pmid: 27237738

ACKNOWLEDGMENTS

We thank H. Friesen, E. Ünal, A. Caudy, and J. Hanchard for discussions and experimental input, and A. Baryshnikova for discussions and critical comments on the manuscript. **Funding:** Supported by NIH grant R01HG005853 (C.B., B.J.A., and C.L.M.), Canadian Institutes of Health Research grants FDN-143264 and FDN-143265 (C.B. and B.J.A.), NIH grants R01HG005084 and R01GM104975 (C.L.M.), and NSF grant DBI\0953881 (C.L.M.). Computing resources and data storage services were partially provided by the Minnesota Supercomputing Institute and the UMN Office of Information Technology, respectively. Additional support was provided by Natural Science and Engineering Research Council of Canada Postgraduate Scholarship–Doctoral PGS D2 (E.K. and A.N.N.B.), a University of Toronto Open Fellowship (E.K.), a University of Minnesota Doctoral Dissertation Fellowship (B.V.), and Deutsche Forschungsgemeinschaft grant CRC1036/TP10 (A.K. and M.K.). C.B. is a fellow of the Canadian Institute for Advanced Research (CIFAR). **Author contributions:** Conceptualization: E.K., B.V., C.L.M., B.J.A., and C.B.; methodology and investigation: E.K., B.V., A.N.N.B., W.W., E.N.K., M.U., A.K., M.M.U., J.v.L., O.K., A.T., M.P., M.-C.H., B.V., M.C., M.K., and A.M.; formal analysis: E.K., B.V., A.N.N.B., W.W., E.N.K., M.U., J.v.L., O.K., A.T., and A.M.; data Curation: M.U.; writing–original draft: E.K., B.V., C.L.M., B.J.A., and C.B.; writing–review and editing: E.K., B.V., A.N.N.B., E.N.K., A.K., M.M.U., J.v.L., A.T., M.C., M.K., A.M., C.L.M., B.J.A., and C.B.; supervision: C.L.M., B.J.A., and C.B.; funding acquisition: C.L.M., B.J.A., and C.B. **Competing interests:** The authors declare no competing interests. **Data and materials availability:** All data associated with this study are available in the supplementary materials. The genetic interaction data are available in a searchable format at http://boonelab.ccbr.utoronto.ca/paralogs/. Tables S1 to S13 were also deposited in the DRYAD Digital Repository (https://doi.org/10.5061/dryad.g79cnp5m9). MATLAB routines that produce SGA digenic and trigenic interaction scores are available at https://doi.org/10.5281/zenodo.3665423.

SUPPLEMENTARY MATERIALS

science.sciencemag.org/content/368/6498/eaaz5667/suppl/DC1
Materials and Methods
Figs. S1 to S9
Tables S1 to S13
References (71–96)
MDAR Reproducibility Checklist

19 September 2019; accepted 6 May 2020
10.1126/science.aaz5667

Exploring whole-genome duplicate gene retention with complex genetic interaction analysis

Elena Kuzmin, Benjamin VanderSluis, Alex N. Nguyen Ba, Wen Wang, Elizabeth N. Koch, Matej Usaj, Anton Khmelinskii, Mojca Mattiazzi Usaj, Jolanda van Leeuwen, Oren Kraus, Amy Tresenrider, Michael Pryszlak, Ming-Che Hu, Brenda Varriano, Michael Costanzo, Michael Knop, Alan Moses, Chad L. Myers, Brenda J. Andrews and Charles Boone

Science **368** (6498), eaaz5667.
DOI: 10.1126/science.aaz5667

The fate of genes after duplication

Gene duplication within an organism is a relatively common event during evolution. However, we cannot predict the fate of the duplicated genes: Will they be lost, evolve, or overlap in function within an organismal lineage or species? Kuzmin *et al.* explored the fate of duplicated gene function within the yeast *Saccharomyces cerevisiae* (see the Perspective by Ehrenreich). They examined how experimental deletions of one or two duplicated genes (paralogs) affected yeast fitness and were able to determine which genes have likely evolved new essential functions and which retained functional overlap, a condition the authors refer to as entanglement. On the basis of these results, they propose how entanglement affects the evolutionary trajectory of gene duplications.

Science, this issue p. eaaz5667; see also p. 1424

Science (print ISSN 0036-8075; online ISSN 1095-9203) is published by the American Association for the Advancement of Science, 1200 New York Avenue NW, Washington, DC 20005. The title *Science* is a registered trademark of AAAS.